Abnormal rolls and regular arrays of disclinations in homeotropic electroconvection

Axel G. Rossberg,[1] Nándor Éber,[2] Ágnes Buka,[2] and Lorenz Kramer[3]

[1]*Department of Physics, Kyoto University, 606-8502 Kyoto, Japan*
[2]*Research Institute for Solid State Physics and Optics, Hungarian Academy of Sciences, P.O. Box 49, H-1525 Budapest, Hungary*
[3]*Institute of Physics, University of Bayreuth, D-95440 Bayreuth, Germany*
(Received 27 September 1999)

We present the first quantitative verification of an amplitude description for systems with (nearly) spontaneously broken isotropy, in particular for the recently discovered abnormal-roll states. We also obtain a conclusive picture of the three-dimensional director configuration in a spatial period doubling phenomenon involving disclination loops. The first observation of two Lifshitz frequencies in electroconvection is reported.

PACS number(s): 47.54.+r, 47.20.Ky, 47.20.Lz, 61.30.Gd

Electroconvection (EC) in thin ($d \sim 10-100 \ \mu$m) layers of nematic liquid crystals (LC) is an important model system for developing and experimentally testing tools for the description of complex, extended pattern-forming systems [1]. In particular, reductive perturbation methods such as the weakly nonlinear amplitude formalism are often employed to describe the behavior slightly above the primary threshold.

EC offers the unique chance to extend the method such that it also captures the secondary instabilities and even the behavior further on, including complex spatiotemporal states. Then, however, not only the (complex) amplitude $A(x,y,t)$ of the convective mode has to be taken into account explicitly, but also the slowly varying in-plane orientation $\hat{c}(x,y,t) = (\cos \varphi, \sin \varphi)$ of the nematic director $\hat{n}(x,y,z,t)$ at midplane ($\hat{c}^2 = 1 = \hat{n}^2$, z axis normal to the LC layer) [2–4].

We consider the common situation where below the threshold of convection $\hat{c}$ is homogeneously oriented along $\hat{x}$ by some external force. This is done either by planar $\hat{n} \| \hat{x}$ surface anchoring [5,6] or, in our case of homeotropic $\hat{n} \| \hat{z}$ anchoring [7,8], by a magnetic field $\vec{H} = \hat{x}H$. As the ac voltage $\sqrt{2} V \sin(2\pi ft)$ applied across the layer is carried through the threshold $V = V_c$ of normal roll (NR) convection, $\hat{c}$ determines the orientation of the wave vector $\vec{q}_c = (q_c, 0) \| \hat{c}$ of the pattern. At a finite distance $(V^2 - V_c^2)/V_c^2 =: \varepsilon > \varepsilon_{AR}$ above threshold, $\hat{c}$ is destabilized by hydrodynamic forces [9,3] exerted by the convection rolls. While the wave vector and the optical appearance of the resulting abnormal rolls (ARs) may remain similar to that of NRs, $\hat{c}$ has now a nonzero angle $\pm \varphi$ with respect to the x axis. This phenomenon is general: it occurs not only in the conduction regime investigated here, but also in the higher-frequency dielectric range [10], as well as in heat induced (Rayleigh-Bénard) convection [5].

The idea of the present work is to keep the AR threshold ε_{AR} small, in order to verify *quantitatively* a recently proposed weakly nonlinear model [2,4]. This is possible in the homeotropic geometry, where, in the limit $H \to 0$, the nematic director acquires its in-plane component ($\hat{n} \neq \hat{z}$) by spontaneously breaking isotropy in a Freedericksz transition at a finite voltage $V_F < V_c$ [7]. Then, for small H^2, $\varepsilon_{AR} \sim H^2$ is small, too.

We describe below an experimental setup for determining the angle φ between $\hat{c}$ and $\hat{x}$, discuss the experimental results and their interpretation in terms of the nonlinear model, and conclude with a brief characterization of the complicated structure we call CRAZY rolls (convection in a regular array of z-y disclination loops), a spatial period doubling phenomenon.

The polarizers in the optical setup [source of parallel white light; polarizer; sample (thermostated at 30 °C); analyzer (removable); long range microscope; charge-coupled-device camera; frame grabber (256 gray levels); PC] could be independently rotated by step motors in steps of 1.8°. Stepping was synchronized to the video frequency, which limited the rotation rate (and the temporal resolution) to 45°/s. The nematic LC Phase 5A (Merck) was used, which contains a dissolved surfactant to ensure the homeotropic alignment. We measure the applied magnetic field $H = 0.32 H_F$ directly in units of the bend Freedericksz threshold $H_F = 2.8$ kOe. Thus the small uncertainty in the (directly measured) cell thickness $d = 31 \pm 1 \ \mu$m is eliminated.

Surprisingly, though in agreement with a numerical stability analysis of the full hydrodynamic equations [9] redone for Phase 5 material parameters (listed in [11]), we find NRs for low frequencies $f < f_{L1} = 180 \pm 30$ Hz and high frequencies $f > f_{L2} = 725 \pm 20$ Hz, while between the two Lifshitz points $f_{L1} < f < f_{L2}$ rolls at the convection threshold are degenerate to two oblique modes [wave vectors $\vec{q}_c = (q_c, \pm p_c)$]. In all previously investigated EC systems, at most one Lifshitz point (f_{L2}) was found. The dielectric regime, for technical reasons, was not accessible in the present experiment.

The only fitting parameter, the conductivity $\sigma_\perp = 8.8 \times 10^{-8} (\Omega \text{m})^{-1}$ was adjusted to match f_{L2} with theory, keeping $\sigma_a/\sigma_\perp = 0.69$ [12] fixed as usual. Absolute values and frequency dependences of experimental threshold voltages and wave numbers agreed with the theory. At low frequencies the observed obliqueness q_c/p_c was larger than predicted (numerically $f_{L1} = 337$ Hz), which is probably an effect of the vicinity of $V_c = O(9 \text{ V})$ and $V_F = 7.48$ V in this range.

Due to the homeotropic anchoring, deviation of $\hat{c}$ from $\hat{x}$ implies a net rotation of the optical axis (no twist, contrary to
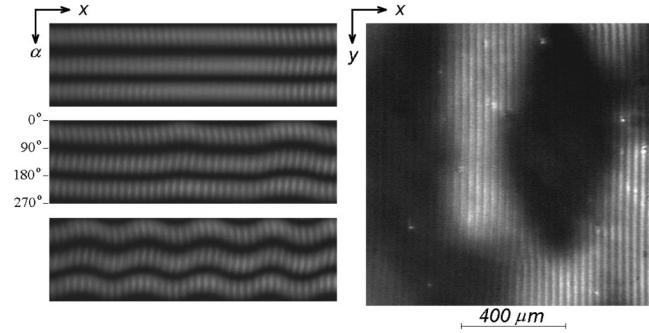
FIG. 1. Snapshot of the AR convection pattern with crossed polars at $\alpha = 8°$ (right-hand side) and a series of x-α maps (left-hand side). $f = 1000$ Hz, $\varepsilon = 0.013$ (upper left), $\varepsilon = 0.027$ (right and middle left), $\varepsilon = 0.040$ (lower left).

the planar case). Thus, two optical effects are superimposed in the recorded images. The focusing/defocusing of the extraordinary beam [i.e., polarizer orientation $\hat{P} := (\cos \alpha, \sin \alpha) \| \hat{c}$] by the periodic tilt modulations of $\hat{n}$ in the roll pattern yields the characteristic stripe pattern (shadow graph, at the selected focus plane the spatial harmonics with wavenumbers $\approx q_c$ dominate over higher harmonics), while, with crossed polarizers only, there is an extinction of all incident light at $\hat{P} \| \hat{c}$ or $\hat{P} \perp \hat{c}$ (dark patches in Fig. 1, right). Although both effects are sensitive to φ, the second one leads to its more accurate determination, while the first effect with parallel polars gave better results for the contrast connected with the pattern amplitude $|A|$.

For a systematic analysis of the state at a given V and f, a single line ($y = $ const) of the video image was recorded as a function of α, with parallel as well as with crossed polars. The resulting x-α maps allow direct visualization of spatial modulations of φ. Figure 1 (left) demonstrates the transition from NRs (straight extinction lines, top left) to ARs with increasing ε. Near ε_{AR} the AR domains possess an irregular "patchy" distribution (middle left and right side of Fig. 1) with slow, persistent dynamics, while at higher ε an almost periodic AR domain structure is preferred (bottom left).

Around each point $x = x_0$ on the line, intervals of a fixed width larger than the pattern wavelength were selected to calculate the average graylevel for crossed, and the difference between the maximum and the minimum graylevel (the variation) for parallel polars. As functions of α an LMS fit to $I_h \sin^2 2(\alpha - \varphi)$ for the average graylevel yields the director orientation $\varphi(x_0)$ [and also $I_h(x_0)$], while from the fit of the variation to $I_p \cos^4(\alpha - \varphi)$ we obtained the quantity $I_p(x_0)$ connected with the pattern amplitude, i.e., with the periodic variations of the tilt angle. This scheme allows absolute measurements of φ with an accuracy of $\pm 2°$.

A typical result for the average of $I_p(x_0)$ over x_0 as a function of ε is shown in Fig. 2(a). Three ranges can be distinguished. The subcritical range ($\varepsilon < 0$), where I_p is dominated by noise, then a relatively fast increase of I_p with ε, up to a voltage that corresponds to $\varepsilon = \varepsilon'_{AR}$ (see below), and a slow decrease for higher voltages. The transition between the subcritical and the increasing range was used to determine the threshold $V = V_c(\varepsilon = 0)$. The uncertainty in V_c due to small imperfections of the sample is a major source of experimental error.
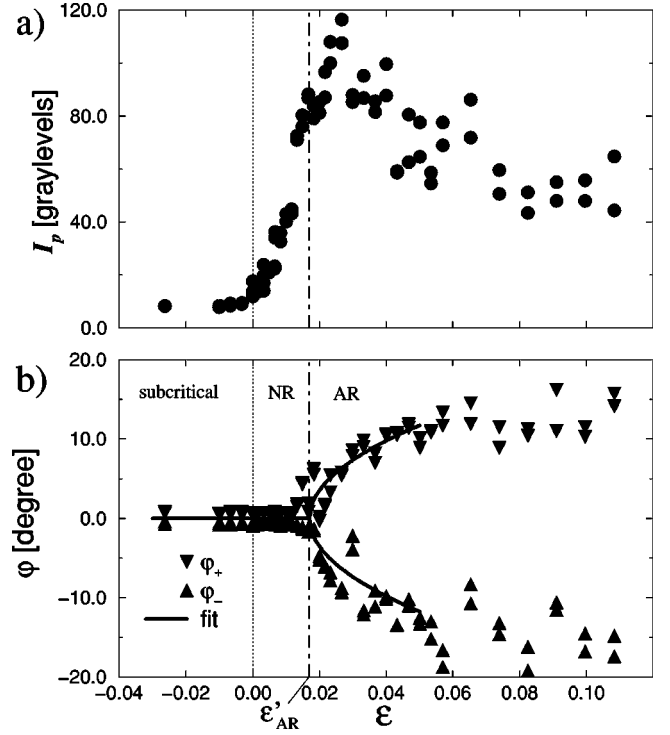

FIG. 2. ε dependence of some pattern characteristics (at $f = 1000$ Hz). (a) I_p (a quantity connected with the pattern amplitude and thus the director tilt). (b) azimuthal angle of the director and fit according to Eq. (1).

The measured values for the maximum φ_+ and minimum φ_- of the director deflection $\varphi(x_0)$ [see Fig. 2(b)] clearly expose a supercritical pitchfork bifurcation at some finite distance ε'_{AR} from threshold. The scatter in the data is mainly due to migration of defects and of domain boundaries. The bifurcation was characterized by fitting (LMS) the function

$$\varphi_{\pm} = \begin{cases} \pm \Phi' \sqrt{\varepsilon - \varepsilon'_{AR}} & (\varepsilon > \varepsilon'_{AR}) \\ 0 & (\varepsilon < \varepsilon'_{AR}) \end{cases} \qquad (1)$$

to the data. The frequency dependence of the fitting parameters ε'_{AR} and Φ' is shown in Figs. 3(a) and 3(b).

We now compare with the relevant predictions of the above mentioned weakly nonlinear description valid for small ε and φ,

$$\tau \partial_t A = [\varepsilon + \xi_{xx}^2 \partial_x^2 + \xi_{yy}^2 (\partial_y^2 - 2iq_c \varphi \partial_y - q_c^2 \varphi^2)$$
$$- g|A|^2 + i\beta_y(\partial_y \varphi)]A, \qquad (2)$$

$$\tilde{\gamma}_1 \partial_t \varphi = [K_1 \partial_y^2 + K_3 \partial_x^2 - \tilde{\chi}_a H^2 - (q_c^2 \Gamma/2)|A|^2]\varphi$$
$$+ (q_c \Gamma/2) \text{Im}\{A^* \partial_y A\} \qquad (3)$$

(all coefficients are real and, except for Γ and β_y, positive; they have been calculated for our material, see [2] for details). For the amplitude $|A|$ of rolls with wave vector $\vec{q}_c = (q_c, p)$ one has $g|A|^2 = \varepsilon - \xi_{yy}^2 [p - q_c \varphi_0(p, \varepsilon)]^2$. Since Γ turns out to be negative for all materials explored so far, $\varphi = \varphi_0(\varepsilon, p)$ is uniquely determined only for small ε. For $p = 0$, there is at $\varepsilon = \varepsilon_{AR} := 2g\tilde{\chi}_a H^2/(|\Gamma| q_c^2)$ a transition (su-
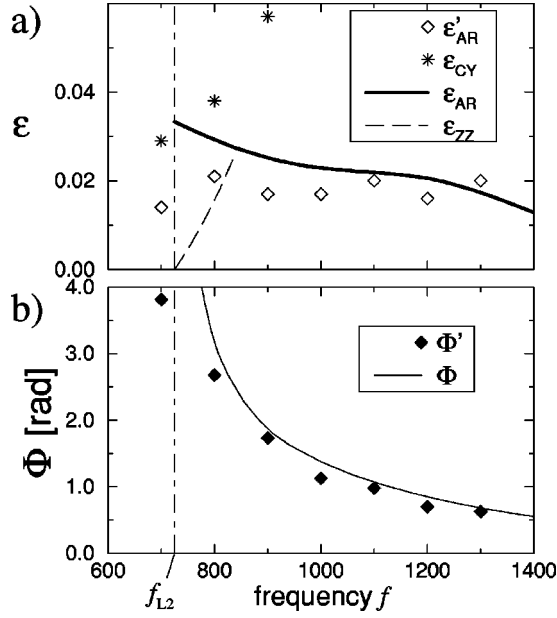
FIG. 3. Frequency dependence of the fit parameters Φ' and ε'_{AR} in formula (1). Solid lines are the corresponding theoretical predictions. Our evaluation scheme gives meaningful results also slightly below f_{L2} (leftmost diamonds) where rolls are only weakly oblique at threshold. Furthermore, the thresholds of CRAZY rolls ε_{CY} (experimental) and of the zig-zag instability ε_{ZZ} for $p=0$ (theoretical) are shown.

percritical pitchfork) from NRs with $\varphi_0=0$ to ARs with $\varphi_0=\pm(\xi_{yy}q_c)^{-1}\sqrt{\varepsilon-\varepsilon_{AR}}$, i.e., Eq. (1) with $\Phi'=\Phi:=(\xi_{yy}q_c)^{-1}$, $\varepsilon'_{AR}=\varepsilon_{AR}$. Remarkably, though ARs are an essentially nonlinear effect, Φ depends only on coefficients relating to the convection threshold. This is a consequence of the rotational symmetry underlying the theory (for $H=0$). The strong increase of Φ for lower frequencies [see Fig. 3(b)] is due to a decrease of ξ_{yy} ($\xi_{yy}\to0$ for $f\to f_{L2}$). The amplitude of abnormal patterns with $p=0$ is $|A|^2=\varepsilon_{AR}/g$ independent of ε in the model, which corresponds to the slow decrease of I_p in Fig. 2(a). For $p\neq0$ the pitchfork becomes imperfect and a saddle-node at $\varepsilon=\varepsilon_{SN}:=\varepsilon_{AR}+3\cdot4^{-1/3}|\xi_{yy}p\varepsilon_{AR}|^{2/3}$ remains. For the new stable branch arising in this bifurcation (for modulation instabilities see below) one has $p/\varphi\geq0$, which we then consider the defining property of ARs. For the continuous ("normal") branch always $p/\varphi<0$.

There are two kinds of long-wavelength modulation instabilities [4,2]. First, an Eckhaus-type instability, which is presumably not relevant for the present experiments, and second, a zig-zag (or undulatory) instability, which destabilizes NRs only if $\beta_y>0$ and $\varepsilon>\varepsilon_{ZZ}:=\varepsilon_{AR}(1+\check{\beta}_y)^{-1}+(1+\check{\beta}_y)^2\xi_{yy}^2p^2\check{\beta}_y^{-2}$, where $\check{\beta}_y=\beta_y/(\xi_{yy}^2q_c)$. As in planar systems [5,3,6], $\varepsilon_{ZZ}\to0$ as $f\to f_{L2}$. If $\beta_y<0$, NRs or ARs with not too large $|p|$ should be stable. Although from the hydrodynamic equations we do find (numerically) $\beta_y<0$ for frequencies $f>f_{AR}=844$ Hz, in the experiments some defects were usually present at all frequencies and voltages. In the stable region they are probably generated at unavoidable inhomogeneities in the sample and not by an intrinsic instability. Effects from the zig-zag instability can be excluded for $f\gtrsim1000$ Hz because in that regime the rolls remain perfectly
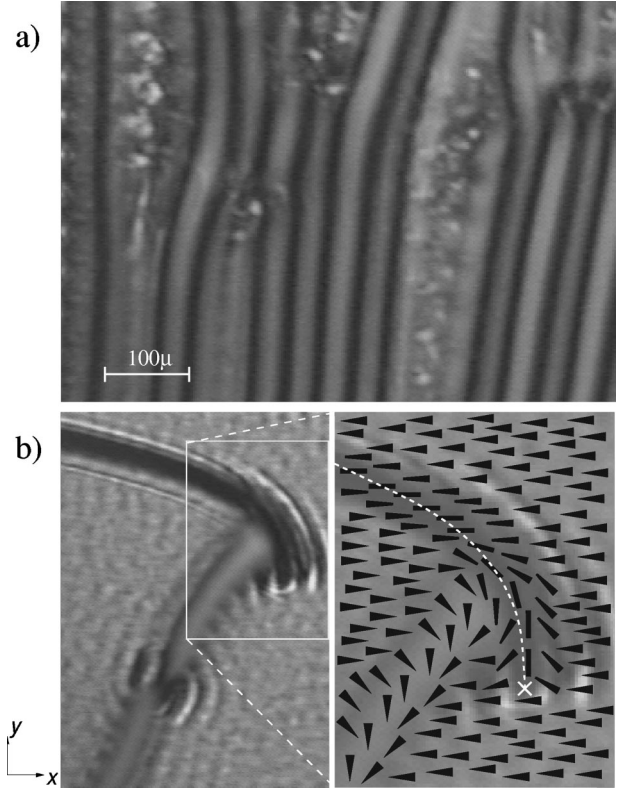

FIG. 4. (a) Snapshot of CRAZY rolls; analyzer and polarizer $||\hat{x}$ ($f=800$ Hz, $\varepsilon=0.060$). (b) Disclination loops and walls near the convection threshold. In the magnification (right) the configuration of $\hat{n}$ at mid plane ("sticks," wide ends pointing upwards), the positions of the sidewall disclinations ($---$), and of the bulk disclination ($\times$) are shown schematically. The 3D director configuration is obtained by interpolating between mid plane and the homeotropic boundaries ($f=800$ Hz, $\varepsilon=-0.010$).

straight when passing through the transition. For lower frequencies some phase modulations were observable which may, however, be connected with the fact that ξ_{yy} is rather small in that range.

The rather large discrepancy between ε'_{AR} and ε_{AR} in Fig. 3(a) near $f=f_{L2}$ is still within the experimental uncertainties. The good match between Φ' and Φ could be slightly fortuitous in view of the fact that Φ relates to regular ARs (at $p=0$), while the experimental AR domains were of finite size and contained defects. Relaxation of φ towards large domains (coarsening) is prevented by the coupling to the phase of the pattern.

When $|\varphi_\pm|$ exceeds $\sim20°-30°$, which we observed only for $f<1000$ Hz, there is a further transition at ε_{CY} [see Fig. 3(a)], which extends also into the oblique-roll range. Disclination loops in the $(y-z)$ plane (CRAZY rolls), appearing as dark lines stretched in $\hat{y}$ direction, propagate into the image [Fig. 4(a)]. Each of them replaces one pair of convection rolls. They may form a periodic structure leaving gaps of width $\approx2\pi/q_c$ between them, but sometimes some loops are left out. Then, either usual convection rolls fill the space, or there is an additional modulation in $\hat{y}$ with a period of $\approx2\pi/q_c$ [Fig. 4(a)].

Using the rotating-polarizer setup we see that $\hat{c}$ rotates by about $\pi/2$ (from $\varphi=-\pi/4$ to $+\pi/4$, or vice versa) at each

loop. In neighboring loops the rotation direction alternates. This doubles the period of the structure ($\approx 4\pi/q_c$) compared to usual convection rolls (a recent, similar observation was interpreted very differently [13]). Since the threshold for the creation of CRAZY rolls is above the EC threshold [Fig. 3(a)] and they disappear for $\varepsilon < 0$, we conclude that the conductive Carr-Helfrich convection mechanism is essential for these structures. This is why we call them CRAZY rolls, in distinction to arrays of disclinations of (presumably) flexo-electric origin [14].

The structure of CRAZY rolls is most easily understood by studying first the slowly relaxing state obtained after the voltage is reduced below the EC threshold; see Fig. 4(b). There are two domains of oppositely tilted Freedericksz deformed states ($\hat{c}$ parallel and antiparallel to $\vec{H}$) separated by different kinds of walls. In the lower part, there is a regular Bloch wall, where $\hat{c}$ rotates around the z axis from one orientation to the other (note the umbilic that separates two symmetry-equivalent variants). In the upper part there is an Ising type wall (mostly twist), where $\hat{c}$ remains along the axis of $\vec{H}$. $\hat{n} \perp \hat{z}$ for all z in the wall center, which requires disclination lines to run along the top and bottom boundary of the sample (which is favored for a weak director anchoring [15], as is probably the case in our sample).

The tip of the disclination loop, which extends slightly beyond the Ising wall [up to the white cross in Fig. 4(b)], has the topology of the essential building block of a CRAZY roll. For higher voltages it evolves continuously towards one of the black lines of CRAZY rolls. It contains both the rotation of $\hat{c}$ from the Bloch wall (though in periodic CRAZY rolls $\hat{c}$ does not rotate all the way to the x axis) and the twist from the Ising wall, and is thus topologically neutral with respect to the $\hat{c}$ field. The complete variation of $\hat{n}$ in midplane when passing through a CRAZY loop is approximately given by a rotation of $\hat{n}$ in some plane parallel to the y axis.

At higher frequencies and with increasing ε_{SN}, chevron-like patterns arise (rather than CRAZY rolls). At small (vanishing) magnetic fields such chevrons can be observed near (at) threshold [16].

In summary, using the rotating polarizer setup we could solve two problems of very different natures: a quantitative test of a highly nontrivial model for pattern formation in anisotropic systems and a clarification of the 3D structure of CRAZY rolls.

[1] L. Kramer and W. Pesch, in *Pattern Formation in Liquid Crystals*, edited by Á. Buka and L. Kramer (Springer-Verlag, New York, 1996).

[2] A. G. Rossberg, A. Hertrich, L. Kramer, and W. Pesch, Phys. Rev. Lett. **76**, 4729 (1996).

[3] E. Plaut and W. Pesch, Phys. Rev. E **59**, 1747 (1999).

[4] A. G. Rossberg, Ph.D. dissertation, University of Bayreuth, 1997 (available upon request).

[5] E. Plaut *et al.*, Phys. Rev. Lett. **79**, 2367 (1997).

[6] S. Rudroff, H. Zhao, L. Kramer, and I. Rehberg, Phys. Rev. Lett. **81**, 4144 (1998).

[7] H. Richter, Á. Buka, and I. Rehberg, Mol. Cryst. Liq. Cryst. Sci. Technol., Sect. A **251**, 181 (1994).

[8] J.-H. Huh, Y. Hidaka, and S. Kai, Phys. Rev. E **58**, 7355 (1998).

[9] A. Hertrich, W. Decker, W. Pesch, and L. Kramer, J. Phys. (Paris) II **2**, 1915 (1992).

[10] H. Amm, R. Stannarius, and A. G. Rossberg, Physica D **126**, 171 (1999).

[11] M. Treiber, N. Éber, Á. Buka, and L. Kramer, J. Phys. (Paris) II **7**, 649 (1997).

[12] In nematics, second rank material tensors have the form $t_{ij} = t_\perp + t_a n_i n_j$; $(n_i) := \hat{n}$.

[13] C. Fradin, P. L. Finn, H. R. Brand, and P. E. Cladis, Phys. Rev. Lett. **81**, 2902 (1998).

[14] H. Hinov and L. Vistin, J. Phys. (Paris) **40**, 269 (1979).

[15] R. B. Meyer, Solid State Commun. **12**, 585 (1973).

[16] A. G. Rossberg and L. Kramer, Physica D **115**, 19 (1998); P. Toth, Á. Buka, J. Peinke, and L. Kramer, Phys. Rev. E **58**, 1983 (1998).